Theory of line shapes for zero field NMR in the presence of molecular motion

P. Meier[a] and G. Kothe
Institut für Physikalische Chemie, Universität Stuttgart, Pfaffenwaldring 55, D-7000 Stuttgart 80, West Germany

P. Jonsen,[b] M. Trecoske, and A. Pines
Department of Chemistry, University of California and Materials and Chemical Sciences Division, Lawrence Berkeley Laboratory, Berkeley, California 94720

(Received 19 May 1987; accepted 21 July 1987)

Dynamic molecular processes modulate dipolar and quadrupolar interactions in nuclear spin systems. Zero field NMR measures evolution arising purely from these interactions, and thus can be used to characterize molecular dynamics in disordered samples. A theory is presented which numerically simulates the effect of molecular reorientation in zero field NMR for a spin-1 nucleus or pairs of dipolar coupled spin-1/2 nuclei. Representative zero field NMR simulations are compared to their high field NMR analogs to demonstrate features which make zero field NMR a potentially useful tool for the study of molecular dynamics.

I. INTRODUCTION

Deuterium high field NMR of isotropic and anisotropic liquids and solids has proved invaluable in the investigation of molecular dynamics.[1–6] In this work, we present a theory which describes the effect of molecular motion on zero field NMR spectra and demonstrates the applicability of this technique in determining the motional model and extracting the relevant dynamic parameters such as jump angles and rates or diffusion axis and constants. High field NMR resonances of those systems arising from intrinsic static orientational anisotropy of the sample are usually broad and often featureless.[3,7,8] These line shapes are determined by molecular motions. However, the deduction of the motional model from these spectra may prove difficult, especially if the effects on the line shape are subtle. Recently, Schmidt *et al.* have demonstrated a two-dimensional ^{2}H NMR experiment which is model independent and yields the jump angle directly from the spectrum.[9]

Zero field NMR spectra of anisotropic liquids and solids contain sharp "crystal" like resonances. These resonances are characterized by the quadrupolar and/or dipolar interaction. Therefore, zero field NMR should be able to exploit the whole dynamic range of the local interaction without the complicated inclusion of the Zeeman interaction. Hennel *et al.* and Jonsen *et al.* have published analytical theories describing systems of two and three dipolar coupled protons,[10] pairs of spin-1/2 nuclei, and isolated spin-1 nuclei.[11] Serebrennikov has developed a compact expression for the zero field spectra of molecules undergoing Brownian reorientations.[12] In this paper we describe numerical solutions of multisite jump and continuous diffusive reorientation in zero field NMR. The methods used in this work are extensions to the analytical zero field approach[11] and previous high field treatments.[4,13] Freed *et al.* have considered earlier the effects of motions on ESR lines of electronic triplet states in zero field.[14] In the following we compare high and zero field NMR with particular reference to dynamic processes, in particular planar jumps, tetrahedral jumps, planar diffusion, and spherical diffusion.

A. Zero field NMR experiment

At present, there are two basic zero field NMR experiments: (a) sudden version and (b) adiabatic demagnetization in the laboratory frame (ADLF). The sudden version involves the preparation of magnetization in first rank tensor operators and ADLF in second rank tensor operators. The experimental methods and apparatus used in these techniques have been described elsewhere.[15–20] The theory described here pertains only to the sudden version of the zero field NMR experiment.

B. Nomenclature and convention

The electric field gradient (EFG) tensor has components V_{ii}, $i = X, Y, Z$, in its principal axis system (PAS). The magnitudes of these three field gradients follow the convention $|V_{ZZ}| \geqslant |V_{YY}| \geqslant |V_{XX}|$. The asymmetry of the EFG tensor is given by $\eta = (|V_{YY}| - |V_{XX}|)/|V_{ZZ}|$ and $V_{ZZ} = \text{eq}$. The quadrupolar coupling constant for a spin-1 nucleus is $A = e^2qQ/(4h)$. For dipolar couplings between two spin-1/2 nuclei, this constant can be replaced with $A = \gamma_i\gamma_j h/(4\pi^2 r_{ij}^3)$ and $\eta = 0$, where γ_i is the gyromagnetic ratio of nucleus i and r_{ij} is the internuclear distance between nucleus i and nucleus j. The units of A are $[s^{-1}]$.

The exchange rate of a jump process is denoted κ_J and a continuous diffusion process is denoted κ_R. The exchange rate is simply the inverse correlation time, properly defined according to the motional model.[3,4] The units of κ are $[s^{-1}]$. The motional regimes are described by the unitless constant κ/A.

C. Assumptions

The assumptions made prior to the theoretical treatment are: (1) the molecular dynamics are stationary Markov processes, (2) the instantaneous jump alters only the

[a] Present address: Laboratorium für Physikalische Chemie, Eidgenössiche Technische Hochschule, 8092 Zürich, Switzerland.
[b] Present address: BP Research Centre, Spectroscopy Branch ASRD, Chertsey Road, Sunbury-on-Thames, Middlesex TW16 7LN, England.

spatial part of the Hamiltonian, no transitions are excited between the nuclear energy levels, and (3) no couplings exist between the sites. Assumption (3) can be easily satisfied in the ^{2}H zero field NMR experiment by using partially deuterated samples.

II. DENSITY MATRIX THEORY

In this section, a dynamic NMR model for $I = 1$ and pairs of dipolar coupled $I = 1/2$ spin systems is developed using the density matrix formalism. The spin Hamiltonian employed considers quadrupolar or dipolar interactions. Evolution and relaxation in zero field are described by the stochastic Liouville equation,[21,22] which is solved using a finite grid point method.[23,24] Diffusive and jump motions are explicitly considered in the calculation. This approach is a direct extension of previous high field[4,13] and zero field[11] treatments.

A. Zero field Hamiltonian

The spin Hamiltonian, representing quadrupolar interactions in the laboratory frame **x, y, z**, defined by the polarizing field B_o, is conveniently written as a scalar product of two irreducible spherical tensors:

$$\mathscr{H}_Q(\Omega) = \sum_{M=-2}^{+2} (-1)^M F_{2,-M}(\Omega) T_{2,M} , \tag{1}$$

where $T_{2,M}$ and $\mathbf{F}_{2,-M}(\Omega)$ denote laboratory frame spin operators

$$\begin{aligned} T_{2,0} &= 6^{1/2}(3I_z^2 - \mathbf{I}\cdot\mathbf{I}) , \\ T_{2,\pm 1} &= \mp (1/2)(I_\pm I_z + I_z I_\pm) , \\ T_{2,\pm 2} &= (1/2) I_\pm I_\pm , \end{aligned} \tag{2}$$

and spatial operators, respectively. In high field, it is usual to neglect the nonsecular terms, $T_{2,M}$ with $M \neq 0$. The orientation dependence of the spatial operators can be evaluated by a twofold transformation from the principal axis system $\mathbf{X}_p$, $\mathbf{Y}_p$, $\mathbf{Z}_p$ in which

$$\begin{aligned} F'_{2,0} &= 6^{-1/2} hA , \\ F'_{2,\pm 1} &= 0 , \\ F'_{2,\pm 2} &= hA\eta , \end{aligned} \tag{3}$$

where A and η are defined in Sec. I B. The zero field Hamiltonian, in its PAS, is explicitly written as follows:

$$\mathscr{H}'_Q = hA\,[6^{-1/2} T_{2,0} + \eta(T_{2,2} + T_{2,-2})] . \tag{4}$$

The Hamiltonian is transformed from the PAS to a molecular, or diffusion, tensor system $\mathbf{X}_M$, $\mathbf{Y}_M$, $\mathbf{Z}_M$, using the Wigner rotation matrix $\mathscr{D}^{(2)}(\phi\theta\psi)$[25] and, finally, into the laboratory frame using $\mathscr{D}^{(2)}(\Phi\Theta\Psi)$, see Fig. 1. The spatial operators are then given by

$$F_{2,M}(\Omega) = \sum_{M',M''=-2}^{+2} \mathscr{D}^{(2)}_{M',M}(\Phi\Theta\Psi)\mathscr{D}^{(2)}_{M'',M'}(\phi\theta\psi) F'_{2,M''} . \tag{5}$$

Diagonalization of the zero field Hamiltonian, Eq. (1), is achieved by the similarity transformation

$$\mathbf{R}^{-1}(\Omega)\cdot\mathscr{H}_Q(\Omega)\cdot\mathbf{R}(\Omega) = \mathscr{H}'_Q , \tag{6}$$

where $\mathscr{H}'_Q$ and $\mathbf{R}(\Omega)$ denote the constant eigenvalues $hA(1 \pm \eta)$, $-2hA$, and the orientation-dependent eigenvectors related to the twofold coordinate transformation [Eq. (5)], respectively.

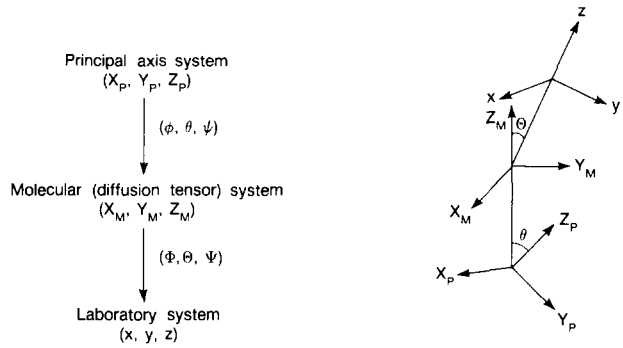

FIG. 1. Notation for coordinate systems and Euler transformations used in the relaxation model. The coordinate systems are: $(\mathbf{X}_P, \mathbf{Y}_P, \mathbf{Z}_P)$, principal axis system for magnetic interaction tensor; $(\mathbf{X}_M, \mathbf{Y}_M, \mathbf{Z}_M)$, molecular axis system with diagonal diffusion tensor; $(\mathbf{x}, \mathbf{y}, \mathbf{z})$, external laboratory system to create the initial condition.

B. Stochastic Liouville equation

Formally, the observable zero field NMR signal obtained from the sudden experiment is given by

$$L(t') = \mathrm{Tr}[\,<\boldsymbol{\rho}(\Omega,t')>\cdot\mathbf{I}_z\,] , \tag{7}$$

where $\boldsymbol{\rho}(\Omega,t')$ is the time-dependent full spin density matrix, assumed to obey the stochastic Liouville equation[21–24]

$$\frac{\partial}{\partial t'}\boldsymbol{\rho}(\Omega,t') = -(i/\hbar)\mathscr{H}^{\times}_Q(\Omega)\cdot\boldsymbol{\rho}(\Omega,t') - \boldsymbol{\Gamma}_\Omega\cdot[\boldsymbol{\rho}(\Omega,t') - \boldsymbol{\rho}_{\mathrm{eq}}(\Omega)] , \tag{8}$$

$\mathscr{H}^{\times}_Q(\Omega)$ denotes a superoperator[26] associated with the zero field Hamiltonian $\mathscr{H}_Q(\Omega)$. $\boldsymbol{\Gamma}_\Omega$ is the stationary Markov operator for the various motional processes with the equilibrium distribution $\mathbf{P}_{\mathrm{eq}}(\Omega)$ obeying

$$\boldsymbol{\Gamma}_\Omega\cdot\mathbf{P}_{\mathrm{eq}}(\Omega) = 0 \tag{9}$$

and

$$\boldsymbol{\rho}_{\mathrm{eq}}(\Omega) = \mathbf{R}(\Omega)\cdot\{(1/3)\mathbf{P}_{\mathrm{eq}}(\Omega)\cdot[\mathbf{E} - (1/kT)\mathscr{H}'_Q]\}\cdot\mathbf{R}^{-1}(\Omega) \tag{10}$$

is the equilibrium density matrix.

C. Stationary Markov operator

In the finite grid point method, the Markov operator is represented by a transition rate matrix $\mathbf{W}(\Omega,\Omega)$, the elements of which give the transition rate between discrete sites of Ω. The values of the transition rates depend upon the model used to describe the motion. For a continuous diffusive process, rotation through a sequence of infinitesimally small angular steps is assumed and the transition rates must satisfy the following[27]:

$$\begin{aligned} &W(\Omega_M,\Omega_{M+1}) + W(\Omega_M,\Omega_{M-1}) = \kappa_R/3\Delta^2 , \\ &W(\Omega_M,\Omega_N)P_{\mathrm{eq}}(\Omega_M) = W(\Omega_N,\Omega_M)P_{\mathrm{eq}}(\Omega_N) , \\ &W(\Omega_M,\Omega_M) = -\kappa_R/3\Delta^2 , \end{aligned} \tag{11}$$

where Δ is the angular separation of adjacent grid points.

Solving Eq. (11), one can establish values for all "diffusive" transition rates in terms of two rotational exchange rates $\kappa_{R\perp}$ and $\kappa_{R\parallel}$, and the equilibrium population $\mathbf{P}_{eq}(\Omega)$ of the sites. $\kappa_{R\perp}$ is the exchange rate for reorientation of the symmetry axis of the diffusion tensor and $\kappa_{R\parallel}$ refers to rotation about it.

In a random jump process, reorientation occurs through arbitrary jumps between various orientations. Consequently, the "jump" transition rates are given by[28]

$$W(\Omega_M,\Omega_N) = \kappa_J [P_{eq}(\Omega_N) - \delta_{MN}] , \tag{12}$$

where κ_J is the jump exchange rate.

D. Numerical evaluation

By introducing the reduced density matrix, defined as follows:

$$\sigma(\Omega,t') = \rho(\Omega,t') - \rho_{eq}(\Omega) , \tag{13}$$

Eq. (8) can be rewritten as

$$\frac{\partial}{\partial t}\sigma(\Omega,t') = -[(i/\hbar)\mathscr{H}_Q^{\times}(\Omega) + \Gamma_\Omega]\cdot\sigma(\Omega,t') , \tag{14}$$

Eq. (14) integrates to

$$\sigma(\Omega,t') = \exp\{-[(i/\hbar)\mathscr{H}_Q^{\times}(\Omega) + \Gamma_\Omega]t'\}\cdot\sigma(\Omega,0) , \tag{15}$$

where $\sigma(\Omega,0)$ is the initial condition of the reduced density matrix at $t' = 0$.

In the sudden zero field NMR experiment, the initial condition results from the sudden switch-off of the intermediate applied field, yielding

$$\rho(\Omega,0) = (1/3)\mathbf{P}_{eq}(\Omega)\cdot(\mathbf{E} - \delta\mathbf{I}_z) . \tag{16}$$

The initial condition of Eq. (16) does not commute with the quadrupole Hamiltonian and is, therefore, nonstationary and evolution under the zero field Hamiltonian is initiated.

The exponent of Eq. (15) can be diagonalized using a similarity transform:

$$\mathbf{S}^{-1}(\Omega)\cdot[-(i/\hbar)\mathscr{H}_Q^{\times}(\Omega) - \Gamma_\Omega]\cdot\mathbf{S}(\Omega) = \Lambda(\Omega) . \tag{17}$$

The matrix $\Lambda(\Omega)$ is diagonal and contains the eigenvalues of the exponent of Eq. (15). Substitution of Eq. (17) into Eq. (15) results in

$$\sigma(\Omega,t') = \mathbf{S}(\Omega)\cdot\exp[\Lambda(\Omega)t']\cdot\mathbf{S}^{-1}(\Omega)\cdot\sigma(\Omega,0) . \tag{18}$$

In a suitable basis the representation of the exponent of Eq. (15) yields a complex-symmetric matrix. Thus, the numerical evaluation of Eq. (18) is readily accomplished by employing the Rutishauser algorithm.[29] Evaluating the trace of $[\langle\sigma(\Omega,t') + \rho_{eq}(\Omega)\rangle\cdot\mathbf{I}_z]$, according to Eq. (7), gives the zero field interferogram $L(t')$. Fourier transformation of $L(t')$ yields the zero field NMR spectrum. The corresponding high field spectrum is obtained by evaluating the same expression with $\mathbf{I}_+$, yielding the signal function for a simple 90° pulse followed by acquisition.

E. Extension to previous zero field treatment

The previous analytical approach to dynamic effects in zero field NMR[11] can be modified to calculate the zero field NMR spectra for arbitrary orientations of the magnetic tensor with respect to the molecular diffusion axis by merely evaluating the frequency matrix elements and performing a further transformation which converts imaginary frequency elements into reals. Expressions for the frequency elements and this transformation are presented in the Appendix. This method yields matrices of dimension eight per site. This is because the magnetization component of T_{00} is dropped as the trace of quadrupolar and dipolar Hamiltonians is zero. This method requires a single diagonalization in the molecular frame. The general theory described earlier produces matrices of dimension nine per site and the diagonalizations are performed in the laboratory frame. The full dimensionality is retained as the theory is applicable to both zero and high field dynamics problems, including continuous diffusive processes.

III. COMPUTATIONAL METHODS

For the jump models, dedicated programs for zero field and high field motions simulations were used, the zero field program based upon the approach of Jonsen *et al.*[11] For the continuous diffusion models, a program package based on the general theory was used to simulate both zero and high field NMR spectra.[13] All program packages were written in FORTRAN 77.

A. Discrete jump simulations

The analytical program of Ref. 11 was used to simulate the motional effects on the spectra for the two-site jump models. The larger site dynamics problems were modeled using the extended numerical approach. Both the dedicated high and zero field NMR programs were executed on a DEC VAX 11/730.

B. Continuous diffusion simulations

The program package based upon the general theory was run on a HP 1000 F series computer (planar diffusion) and on a CRAY 2 computer of the Computer Center, Universität Stuttgart (spherical diffusion).

C. Computer simulation parameters

Calculations were done for powder samples, e.g., an isotropic distribution for the molecular system with respect to the external laboratory frame was considered. In the case of a static powder (jump motion) the number of grid points in the Euler angle spheres was a function of $\sin(\Theta)$ to efficiently use computing time. In case of a dynamic powder distribution (diffusive motion) the number of grid points was subsequently increased until convergence of the calculated line shapes was achieved. The final number of sites per sphere varied with the value of the exchange rate, a typical value being 25.

All displayed spectra were underlayed with a residual line broadening $\alpha = A/100$.

IV. SIMULATIONS

Here are presented the zero and high field dynamic NMR simulations for some representative motional models. The models considered include both discrete jumps and continuous diffusion. They are planar jumps (two and three sites), tetrahedral jumps (equal and unequal populations), and planar and spherical diffusion.

A. Discrete jump processes

The Euler angles which are the arguments of the Wigner rotation matrix used to make the transformation of the PAS into the molecular diffusion frame are ϕ, θ, and ψ. For planar jumps the jump angle is $\psi = 360°/\text{number of sites}$. The angle θ is the angle between $\mathbf{Z}_P$ and the molecular axis $\mathbf{Z}_M$ (see Fig. 1). ϕ determines the orientation of the $\mathbf{X}_P$ and $\mathbf{Y}_P$ axes. If $\phi = 0°$ then the $\mathbf{Y}_P$ axis is in the plane of rotation. $\mathbf{X}_P$ is in this plane if $\phi = -90°$.

1. Two-site jumps

The two models discussed here are for $\psi = 180°$, $\phi = -90°$, and $\theta = 125.3°$ and 161.4°. These models pertain to the jump motions of water molecules in crystalline hydrates[30–32] and the exchange of hydrogen bonded protons in centrosymmetric carboxylic acid dimers,[33] respectively.

a. $\theta = 125.3°$. Only the rapid and rigid motional regimes have been accessible to NQR,[30,31] whereas ^{2}H NMR has been used to study the entire motional range.[32] Figure 2 depicts the zero and high field NMR spectra, for every motional regime, predicted for a deuteron in a crystalline water molecule which is hopping between two equivalent sites. The asymmetry of the rigid EFG tensor is assigned a value $\eta = 0.1$, this value being typical for static crystalline water molecules.[34] When molecular motion begins to average the quadrupolar interaction, the zero field lines broaden. This broadening is at a maximum in the intermediate motion regime, $\kappa_J/A = 1$. As the exchange rate increases, sharp resonances appear at frequency positions characterized by the tensor values of the time-averaged quadrupole coupling tensor. With the parameters listed here, the effective asymmetry parameter obtained, in the rapid motional limit, is $\eta_{Av} \approx 0.8$. This value is similar to that observed experimentally.[30,31] The high field spectra remain broad over the entire motional regime, no appreciable differences in the spectra being observable for $\kappa_J/A \geqslant 3$. The asymmetry parameter is not as easily determined from the high field spectra compared to the zero field analog. It is apparent from Fig. 2 that the zero field NMR spectra display more pronounced changes compared to the high field NMR spectra.

b. $\theta = 161.4°$. This model pertains to two dipolar coupled protons which are each hydrogen bonded to the carboxylic acid group of the other in a centrosymmetric dimer. Molecular dynamics of this kind have been investigated for the carboxylic acid protons in toluic acid.[33] The static regime in this system, toluic acid, may not be attainable as tunneling effects may become dominant at lower temperatures.

The change in direction of the internuclear vector, arising from a concerted jump of the protons, is 37.2°. Figure 3 illustrates the high and zero field simulated NMR spectra for this model in the motional regimes $0 \leqslant \kappa_J/A \leqslant 10^4$. The dipolar Hamiltonian gives three lines, for the zero field simulation, in the rigid regime at ν_x, $\nu_y = 3A$, $-3A$ and $\nu_z = 0$. As the motion increases, the dipolar interaction is partially averaged and the lines broaden. With κ_J/A values greater than 3, a small asymmetry is observed. In the rapid motional limit, this asymmetry is $\eta_{Av} \approx 0.2$. The high field simulations exhibit little change between the rigid to intermediate and the intermediate to rapid motional regimes. The most pronounced spectral changes occur between $0.1 \leqslant \kappa_J/A \leqslant 3$. The zero field NMR experiment provides a significantly more sensitive technique over a broader range of κ_J/A.

2. Three-site jumps

For the simulations presented here $\psi = 120°$. The other parameters for the models are: (a) $\theta = 90°$, $\phi = 0°$ or $-90°$, $\eta = 0$, (b) $\theta = 90°$, $\phi = -90°$, $\eta = 0.1$, (c) $\theta = 109.4°$,

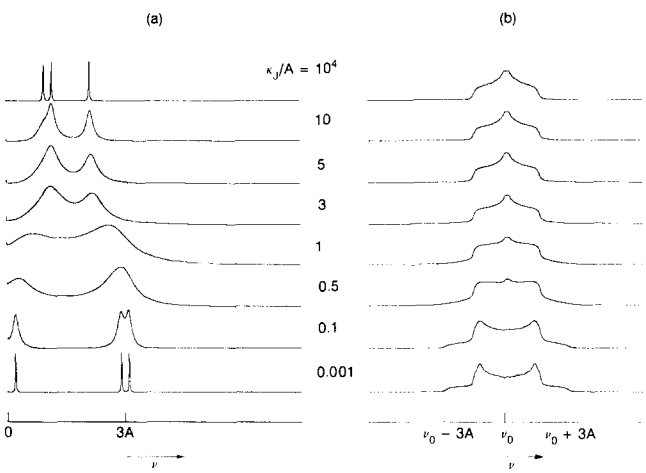

FIG. 2. Computed zero field (a) and high field (b) powder NMR spectra for two-site jumps, $\theta = 125.3°$, in the dynamic range $0.001 \leqslant \kappa_J/A \leqslant 10^4$, $\eta = 0.1$.

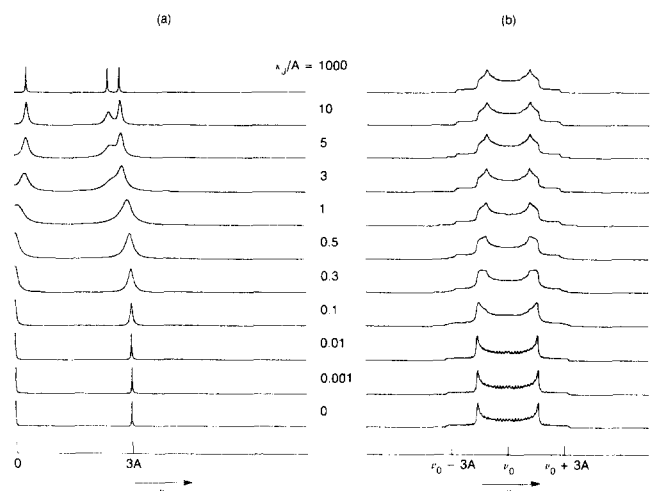

FIG. 3. Computed zero field (a) and high field (b) powder NMR spectra for two-site jumps, $\theta = 161.4°$, in the dynamic range $0 \leqslant \kappa_J/A \leqslant 1000$, $\eta = 0$.

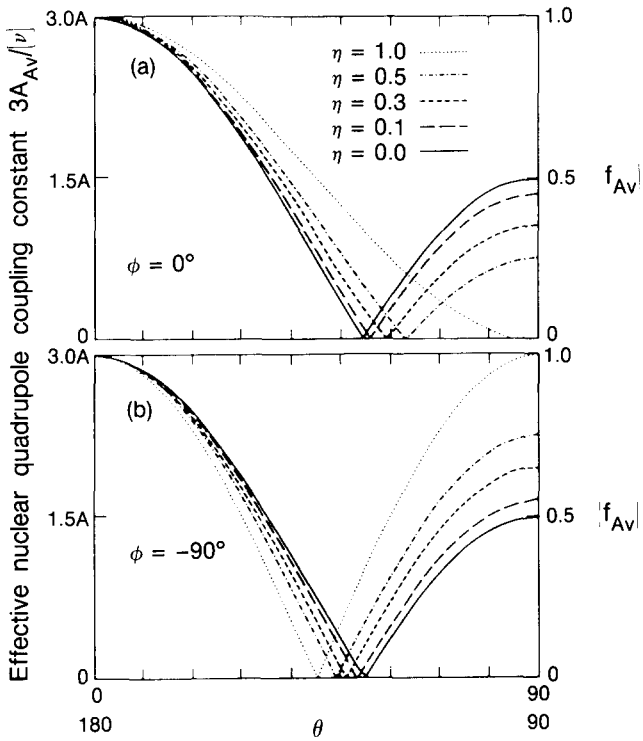

FIG. 4. Computed values of the value of $3A_{Av}$, in terms of the rigid quadrupole coupling, for various rigid asymmetry parameters with respect to the angle θ: (a) $\phi = 0°$; (b) $\phi = -90°$. The magnitude value of the scaling factor of the quadrupole coupling is on the right of the plots.

$\phi = 0°$, $\eta = 0$, and (d) $\theta = 144.7°$, $\phi = 0$, $\eta = 0$. Figure 4 illustrates the dependence of the rapid motionally averaged quadrupole coupling, A_{Av}, for various rigid asymmetry parameters with respect to the angle θ. Figure 4(a) is for $\phi = 0°$ and Fig. 4(b) is for $\phi = -90°$. These results were calculated via the zero field program and agree with those calculated analytically by a weighted time average of the EFG tensors of each site. The relevance of these plots will be discussed below.

a. $\theta = 90°$, $\eta = 0$. These parameters describe the reorientation of $\mathbf{Z}_P$ and $\mathbf{Y}_P$ in the rotation plane and $\mathbf{X}_P$ coincident with the molecular diffusion axis. Figure 5 presents the NMR spectra predicted for the motional range $0.01 \leqslant \kappa_J/A \leqslant 100$ for both zero and high field.

The singularities of the high field spectra broaden as the motional rate approaches $\kappa_J/A = 1$ and then sharpen to yield a powder pattern with $\eta_{Av} = 0$ and $A_{Av} = 0.5A$. The zero field NMR spectra give effective quadrupole coupling constants and asymmetry parameters in total agreement with the high field case. The ν_x and ν_y lines, $\pm 3A$, broaden and begin to shift towards the center of the spectrum, $\kappa_J/A < 1$. The ν_z line (at zero frequency) simultaneously broadens and begins to split. The ν_x and ν_y lines become the effective ν_z^{Av} line in the rapid limit and, conversely, the ν_z line becomes the ν_x^{Av} and ν_y^{Av} lines. In the motional range $1 \leqslant \kappa_J/A \leqslant 3$, the ν_x and ν_y lines are so broad they cannot be observed. For $\kappa_J/A \geqslant 10$, the ν_x and ν_y lines begin to sharpen and show intensity in the center of the spectrum as ν_z^{Av}. At $\kappa_J/A = 100$, the intensities are not yet equal, the motion not yet totally in the rapid motional regime. The rigid ν_z line

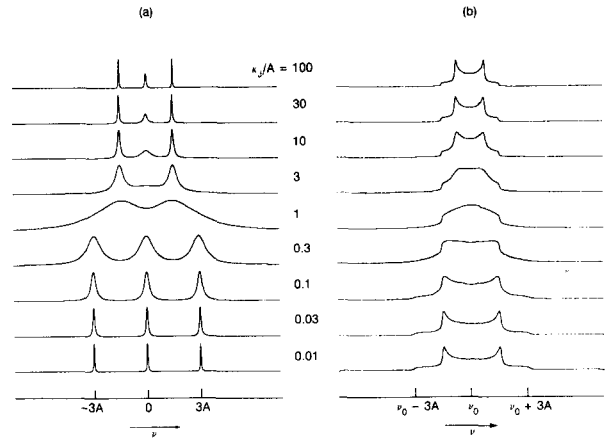

FIG. 5. Computed zero field (a) and high field (b) powder NMR spectra for three-site jumps, $\psi = 120°$, $\theta = 90°$, $\phi = 0°$, $\eta = 0$ and for the dynamic range $0.01 \leqslant \kappa_J/A \leqslant 100$.

does not shift as far as the rigid ν_x and ν_y so it does not broaden to the same extent. Separation of the ν_x and ν_y lines from the ν_z lines can be achieved by using a correctly oriented single crystal.

The spectra given in Fig. 5 are identical to those obtained for six-site exchange, $\psi = 60°$, $\theta = 90°$, and $\phi = 0°$ for both high and zero field NMR. Therefore, the spectra presented in Fig. 5 are relevant to jump rotations of benzene and hexamethyl benzene about their symmetry axis.

b. $\theta = 90°$, $\eta = 0.1$. This model is equivalent to that in *a*, except $\eta = 0.1$. The simulated zero and high field ^{2}H NMR spectra, for $0.01 \leqslant \kappa_J/A \leqslant 100$, are presented in Fig. 6. The asymmetry is averaged to zero by the rotation and the principal axis of the EFG tensor, in the rapid limit, is coincident with the molecular axis $\mathbf{Z}_M$. The individual lines broaden and shift in a similar manner described in the previous section [see Fig. 5(a)]. However, for $\eta = 0.1$, it is possible to discern ν_z^{Av} for $\kappa_J/A = 3$, this extremely broad resonance arising from the rigid ν_x and ν_y resonance. The effective

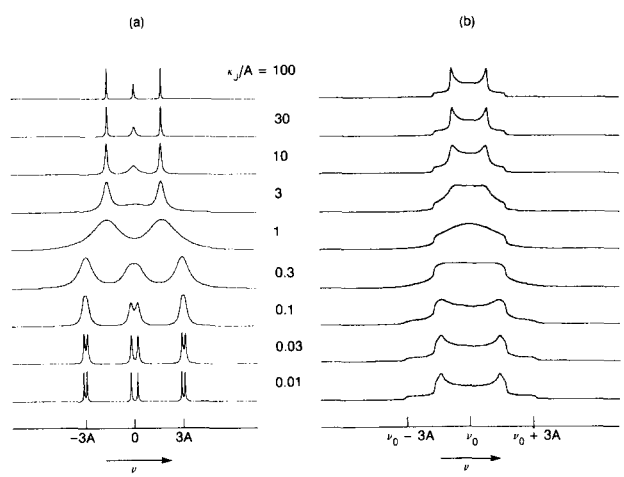

FIG. 6. Computed zero field (a) and high field (b) powder NMR spectra for three-site jumps, $\psi = 120°$, $\theta = 90°$, $\phi = -90°$, $\eta = 0.1$ and for the dynamic range $0.01 \leqslant \kappa_J/A \leqslant 100$.

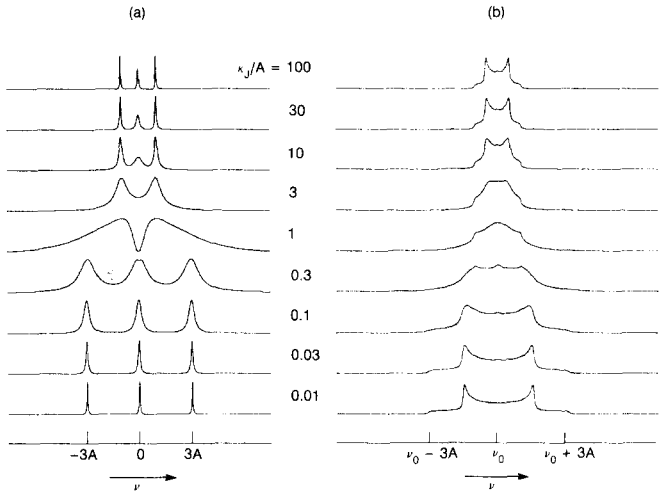

FIG. 7. Computed zero field (a) and high field (b) powder NMR spectra for three-site jumps, $\psi = 120°$, $\theta = 109.4°$, $\phi = 0°$, $\eta = 0$ and for the dynamic range $0.01 \leqslant \kappa_J/A \leqslant 100$.

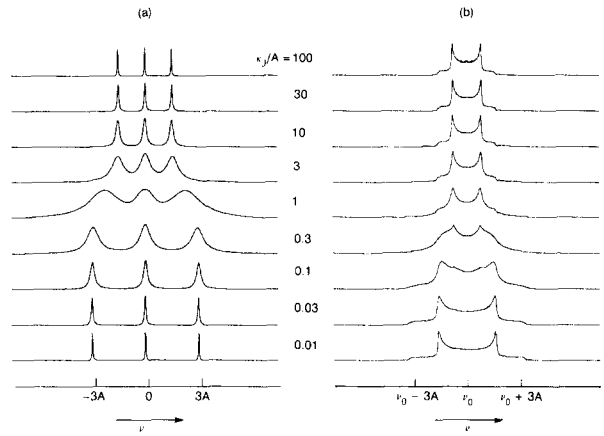

FIG. 8. Computed zero field (a) and high field (b) powder NMR spectra for three-site jumps, $\psi = 120°$, $\theta = 144.7°$, $\phi = 0°$, $\eta = 0$ and for the dynamic range $0.01 \leqslant \kappa_J/A \leqslant 100$.

quadrupole coupling is larger than that obtained for $\eta = 0$, its value being $3A_{Av} = 1.6A$ [see Fig. 4(b)].

c. $\theta = 109.4°$, $\eta = 0$. Figure 7 depicts the zero and high field NMR simulated spectra for the motional range $0.01 \leqslant \kappa_J/A \leqslant 100$. This model can be used to describe the jump of a methyl deuteron between equivalent sites.[30] The effects of the motion are similar to those observed in Fig. 5. However, the value of A_{Av} is much smaller than that in Fig. 5. Therefore, the ν_z resonance does not have to shift as far as in Fig. 5 and remains sharper in the intermediate regime. The ν_z line begins to split at $\kappa_J/A = 0.3$. At $\kappa_J/A = 1$, the ν_x and ν_y lines are very broad but centered at higher frequencies than the ν_z resonances. This gives the component of the doublet an asymmetric appearance with a sharp edged minimum in the center of the spectrum. At $\kappa_J/A = 3$, the rigid ν_x and ν_y resonances have intensity in the center of the spectrum as ν_z^{Av} and this steep edged feature is not present. Such a feature should easily be distinguished, even in the broad spectrum. The zero field NMR simulations display much more pronounced changes, compared to their high field analogs, over the motional range.

d. $\theta = 144.7°$, $\eta = 0$. Figure 8 depicts the simulated zero and high field NMR spectra for $\theta = 144.7°$. For this value of θ and η, it can be realized from Fig. 4 that the value of A_{Av} will be identical to that for $\theta = 90°$ and $\eta = 0$. However, the spectra of Fig. 8 differs from the corresponding spectra in Fig. 5 for the intermediate motional regime. These differences arise from the shifts of the ν_x, ν_y, and ν_z resonances as κ_J/A increases. In this case the ν_x and ν_y lines become the ν_x^{Av} and ν_y^{Av} lines and the ν_z line becomes the ν_z^{Av} line. Therefore, no sharp edged minimum is observed at the center of the spectrum. The intermediate regime is obviously useful in the determination of which side of the magic angle (θ_M, where $A_{Av} = 0$) θ is for the range $90° \leqslant \theta \leqslant 144.7°$.

3. Tetrahedral jumps

Two examples of tetrahedral jumps are presented. These are: (a) equally populated sites and (b) unequally populated sites. These situations give rise to totally different rapid regime results.

a. Isotropic tetrahedral jumps. Figure 9 illustrates the zero and high field NMR spectral simulations for $0.01 \leqslant \kappa_J/A \leqslant 100$. This motional model averages the quadrupole coupling to zero. Hence, only a sharp line at zero frequency is observed in both the zero and high field spectra. The zero field NMR spectra broaden as κ_J/A is increased from the static regime. The resonances then coalesce at the center frequency and sharpen as the exchange rate approaches the rapid motional limit. The high field NMR spectra change as follows: (1) the singularities broaden, (2) at $\kappa_J/A = 0.1$, a peak appears at zero frequency becoming more dominant as κ_J/A increases, and (3) the broad base loses intensity and a single line is resolved in the center of the spectrum. The zero field NMR spectra exhibit far broader lines in the intermediate range than the high field analog. However, in the rapid motional limit, the linewidths of these

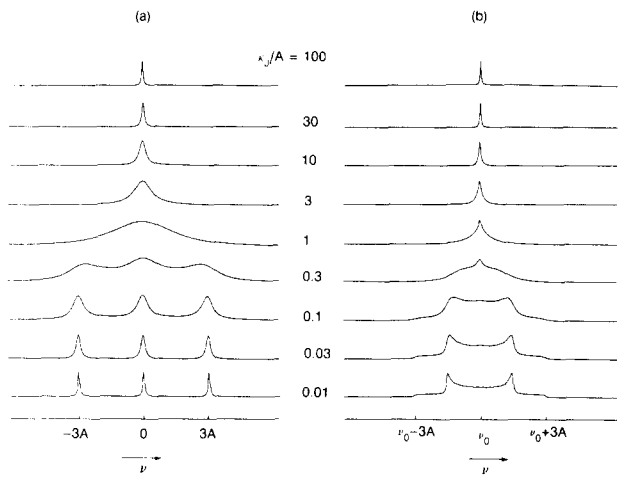

FIG. 9. Computed zero field (a) and high field (b) powder NMR spectra for isotropic tetrahedral jump motion in the dynamic range of $0.01 \leqslant \kappa_J/A \leqslant 100$. $\eta = 0$ and the relative populations of the tetrahedral sites are $P(\Omega_i) = 0.25$, $i = 1, 2, 3, 4$.

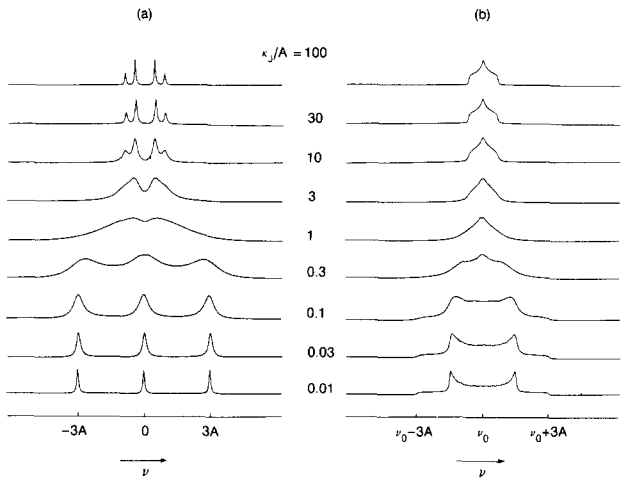

FIG. 10. Computed zero field (a) and high field (b) powder NMR spectra for anisotropic tetrahedral jump motion in the dynamic range of $0.01 \leqslant \kappa_J/A \leqslant 100$. $\eta = 0$ and the relative populations of the tetrahedral sites are $P(\Omega_1) = 0.1$, $P(\Omega_2) = 0.2$, $P(\Omega_3) = 0.3$, and $P(\Omega_4) = 0.4$.

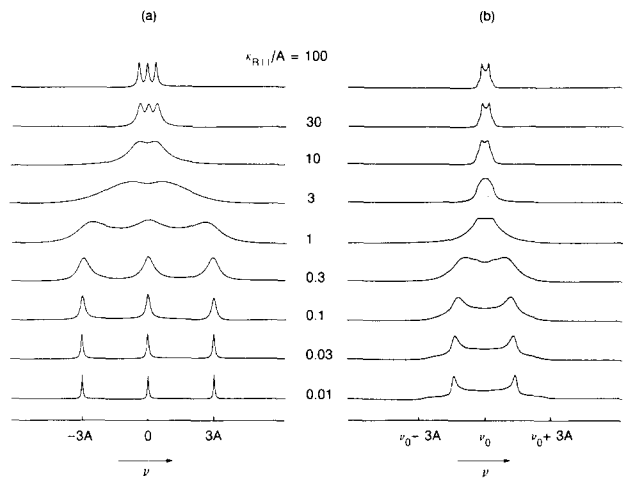

FIG. 12. Computed zero field (a) and high field (b) powder NMR spectra for planar rotational diffusive motion in the dynamic range of $0.01 \leqslant \kappa_{R\parallel}/A \leqslant 100$. $\eta = 0$ and $\theta = 60°$.

two lines should be comparable. As the line narrowing is greater in zero field, one would predict the zero field experiment to be more sensitive in determining exchange rates above the intermediate regime.

Examples of tetrahedral motions include the four ^{14}N nuclei and the three interpenetrating sets of tetrahedrally arranged ^2H nuclei in hexamethylene tetramine.[36,37] The work of Alexander *et al.*[36] considered spin–lattice relaxation of the ^{14}N nuclei in the intermediate regime, where they found the spin-lattice relaxation rate is equal to the exchange rate.

b. Anisotropic populations with tetrahedral jump. Figure 10 depicts the simulated zero and high field NMR spectra for $0.01 \leqslant \kappa_J/A \leqslant 100$ with unequal site populations. For the parameters chosen here, the rapid motionally averaged quadrupole coupling has an asymmetry parameter $\eta_{Av} = 1$. The zero and high field NMR line shape of the rapid motional regime is characteristic of these averaged quadrupole parameters. For values of $\kappa_J/A \leqslant 0.3$, the linewidths of the zero field NMR spectra are far more sensitive than the corresponding high field analogs in the same ways as discussed for Sec. IV A 3 *a*.

B. Continuous diffusion

1. Planar rotational diffusion

This motion refers to a rotation about the symmetry axis of the diffusion tensor. The orientation of the rotation axis is fixed within the laboratory reference frame. Furthermore, an isotropic equilibrium distribution $\mathbf{P}_{eq}(\Omega)$ is assumed. Different orientations of the magnetic tensor with respect to the diffusion tensor have been selected. These orientations are specified by the angle Θ. The different series of zero and high field spectra are shown in Figs. 11–14. This motion yields a fast motion spectrum with $\eta_{Av} = 0$, which is identi-

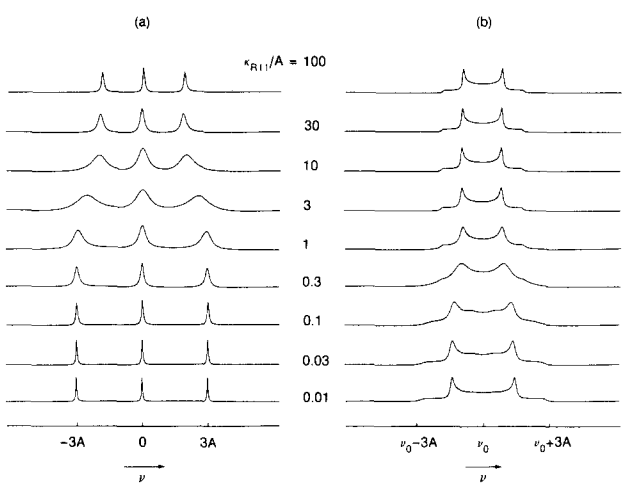

FIG. 11. Computed zero field (a) and high field (b) powder NMR spectra for planar rotational diffusive motion in the dynamic range of $0.01 \leqslant \kappa_{R\parallel}/A \leqslant 100$. $\eta = 0$ and $\theta = 30°$.

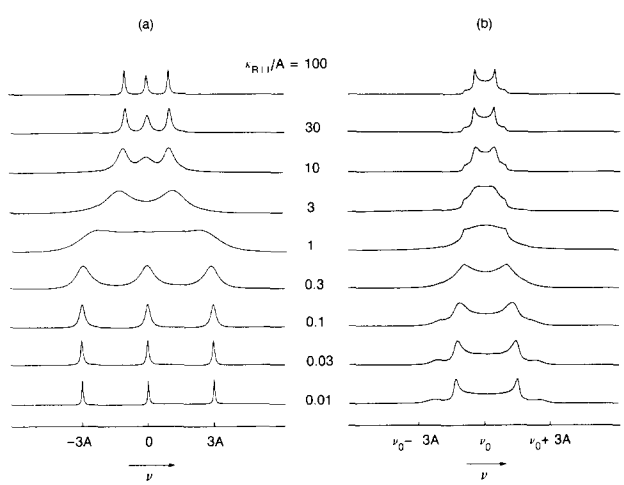

FIG. 13. Computed zero field (a) and high field (b) powder NMR spectra for planar rotational diffusive motion in the dynamic range of $0.01 \leqslant \kappa_{R\parallel}/A \leqslant 100$. $\eta = 0$ and $\theta = 70.6°$.

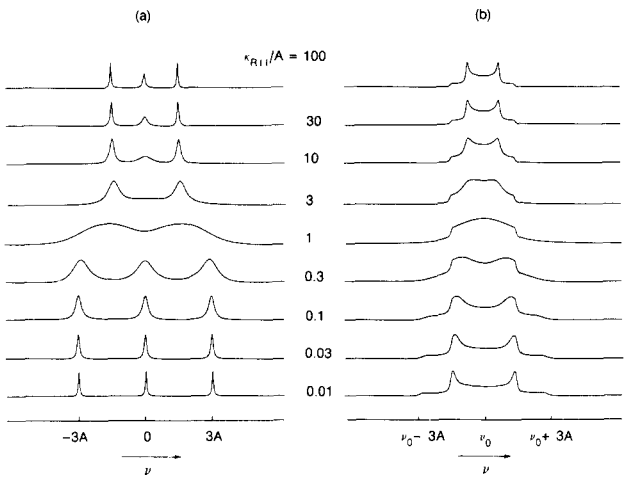

FIG. 14. Computed zero field (a) and high field (b) powder NMR spectra for planar rotational diffusive motion in the dynamic range of $0.01 \leqslant \kappa_{R\|}/A \leqslant 100$. $\eta = 0$ and $\theta = 90°$.

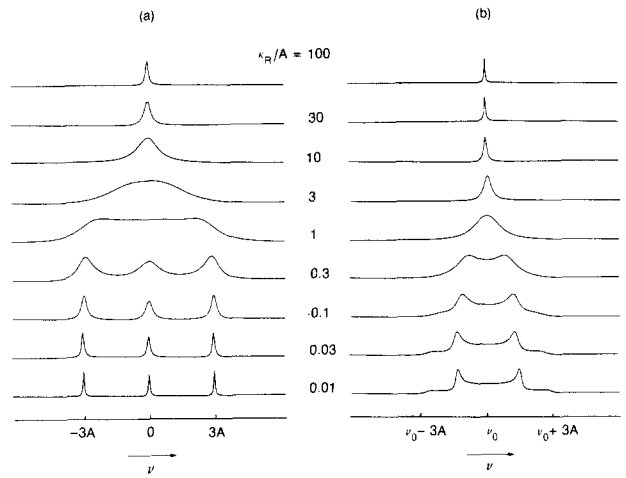

FIG. 15. Computed zero field (a) and high field (b) powder NMR spectra for spherical rotational diffusive motion in the dynamic range of $0.01 \leqslant \kappa_{R\|}/A \leqslant 100$. $\eta = 0$.

cal to the rigid limit spectrum scaled by a frequency factor $f_{Av} = (1/2)(3\cos^2\theta - 1)$. For $\theta <$ arc $\cos[(1/3)^{1/2}]$, the zero field lines do not cross in the intermediate motion regime (Fig. 11), whereas for $\theta >$ arc $\cos[(1/3)^{1/2}]$, they do cross yielding characteristic broad spectral patterns (Figs. 12–14). The situation in high field is similar but more involved since there is always an overlap between the two lines according to the frequency spread of $\pm (3/2)A(3\cos^2\Theta - 1)$ arising from the spatial anisotropy. The different geometrical situations chosen here are relevant for rotational diffusion of alkyl chains and phenyl groups when dealing with deuterons or dipolar coupled protons.

2. Isotropic spherical diffusion

This motion completely averages any second rank tensorial magnetic interaction when the motion is rapid, giving rise to a single zero frequency and a single Larmor frequency line in zero and high field NMR, respectively (see Fig. 15). On decreasing the exchange rate, one sees three lines emerging from the broad coalescence region in zero field, whereas the high field case will gradually change to the rigid limit Pake pattern. These situations arise when symmetric molecules such as deutero-chloroform continuously diffuse in an isotropic environment.

V. DISCUSSION AND CONCLUSIONS

A. Two-site jumps

The linewidths of the resonances for the intermediate motional regime for $\theta = 161.4°$ (see Fig. 3) are much narrower than those in the same regime for $\theta = 125.3°$ (see Fig. 2). In the $\theta = 125.3°$ model, there is a resonance line crossing where the rigid $\nu_z = 2A\eta$ becomes the rapid regime $\nu_y^{Av} = (3 - \eta_{Av})A_{Av}$ resonance and the $\nu_y = (3 - \eta)A$ resonance moves to the $\nu_z^{Av} = 2A_{Av}\eta_{Av}$ position. These changes involve large frequency shifts in which the resonance must broaden to the extent of the frequency difference. The larger the frequency shift, the larger the broadening. This broadening may be different for each individual resonance line. This implies that each resonance line, or component of magnetization, has its own characteristic relaxation time. The resonances in the zero field NMR spectra for $\theta = 161.4°$ and $\kappa_J/A = 1$ are narrower as the frequency shifts are smaller. The different relaxation times are apparent in the zero field NMR spectra for $3 \leqslant \kappa_J/A \leqslant 10$ in Fig. 3. Each line arises from a component of magnetization, g_{kq}, as described in Ref. 11. In the rigid regime, the sudden experiment gives the frequencies: $2^{1/2}g_{10} \equiv \nu_z$; $g_{1-} \equiv \nu_x$; $g_{1+} \equiv \nu_y$. It is expected, therefore, that each of the eight components of magnetization may have a characteristic relaxation time. Different relaxation times should, therefore, be recorded by appropriate choice of the preparation and detection conditions.[17–20] Analysis can be simplified by the use of an oriented single crystal. Zero field NMR is a technique that can measure the spin relaxation of particular components of magnetization. Relaxation in zero field will be considered in greater detail in a future publication.[35]

B. Planar jumps and planar continuous diffusion

We now discuss zero field NMR simulations with $\psi = 360°/n$, $\theta = 90°$ for $n = 4, 5, 6, 10$. In all cases, identical asymmetry parameters and quadrupole couplings were used and, as expected, identical averaged quadrupole parameters were obtained for the rapid motional limit. The high field spectra exhibit minor differences in the intermediate motional regime, however, no such differences were observed for their zero field analogs. All zero field simulations give identical spectra at different exchange rates for different values of n. This suggests that zero field NMR may not be able to determine the numbers of sites in the plane for $\theta = 90°$. Spectra in Fig. 5 have already been described as being identical to the spectra for $n = 6$. Comparison of Fig. 5 with Fig. 14 which is for planar diffusion yields a surprising result. Both the zero field and high field NMR spectra in Fig. 14 are identical to their corresponding spectra in Fig. 5. This implies that both zero field NMR and high field NMR cannot

distinguish between three-site jump ($\psi = 120°$), six-site jump ($\psi = 60°$), and planar diffusion. Of course the two-dimensional NMR experiment of Schmidt *et al.* could be successfully used to determine between the jump process and the continuous diffusion process.[9] Other 1D techniques such as the quadrupolar echo or spin alignment experiment[2,13] could also be used. Dipolar coupling of adjacent deuterons may give additional spectral features, the dipolar coupling being sensitive to the relative orientations of the EFG tensors.[34,38] However, the dimension of the calculations increases rapidly and will not be discussed here. The insensitivity of zero field NMR for multisite exchange processes is not found for $\theta \neq 90°$, as will be seen below.

For $\theta \neq 90°$, some interesting results are found. In Figs. 5 and 6, $\theta = 90°$; Fig. 7, $\theta = 109.4°$; Fig. 8, $\theta = 144.7°$; Fig. 11, $\theta = 30°$; Fig. 12, $\theta = 60°$; Fig. 13, $\theta = 70.6°$ important features are observed which can be explained by referring to Fig. 4. For Figs. 5, 6, 7, 12, and 13 the ν_x and ν_y lines cross ν_z to become the ν_z^{Av} lines. The opposite situation is true for ν_z which becomes the ν_x^{Av} and ν_y^{Av} lines. For Figs. 8 and 11 the rigid ν_x and ν_y lines do not cross with ν_z. This can be simply explained. For $\eta = 0$, the scaling parameter $f_{\mathrm{Av}} = (1/2)(3\cos^2\theta - 1)$. Figure 4 also gives the absolute value of f_{Av} as a function of θ. When f_{Av} is negative the lines cross. Conversely, when f_{Av} is positive the lines do not cross. Such an effect can also be observed in the high field spectra. The Pake patterns consist of two broad lines, denoted ν_+ and ν_-. The frequency spread of these lines is given by $+(3/2)A(3\cos^2\Theta - 1)$ for ν_+ and $-(3/2)A(3\cos^2\Theta - 1)$ for ν_-. For Figs.5–7, 12, and 13 where the ν_x and ν_y lines cross with the ν_z lines, the high field ν_+ and ν_- lines become the averaged ν_-^{Av} and ν_+^{Av} lines, respectively. For these cases the spectra are broad humps in the intermediate regime. For Figs. 8 and 11, the ν_+ line is averaged into the ν_+^{Av} line and the same for ν_-. Therefore, the intermediate spectra in high field retain an appearance of a broad powder pattern, the xy singularities observable throughout the entire motional range. The determination of the value of θ, as it can be realized from Fig. 4 that two values of θ can produce the same value of A_{Av}, is more easily carried out in zero field due to the high resolution character of the spectra.

Comparison of Fig. 7, three-site jumps for $\psi = 120°$, $\theta = 109.4° \equiv 70.6°$, $\phi = 0°$, with Fig. 13, $\theta = 70.6°$, give very similar spectra for the high field regime. The zero field NMR spectra in the intermediate range are, however, very different. The sharp edged minimum at the center of the spectrum of the jump case is not visible in the planar diffusion case. Also, in Fig. 13, no splitting has begun for $\kappa_{R\parallel}/A = 3$ compared to that in Fig. 7 for $\kappa_J/A = 3$. The zero field NMR technique should, therefore, prove invaluable in distinguishing between jump motions or continuous diffusion for $\theta \neq 90°$.

C. Tetrahedral jumps and spherical continuous diffusion

Figures 9 and 15 are of the tetrahedral jump and the continuous spherical diffusion spectra. The high field NMR spectra of these two processes are very different. All the spectra in these figures give a single line at the center of the spectrum for $\kappa/A = 100$. The zero field spectra have more pronounced changes as they start, in the rigid regime, with sharp lines, broaden and coalesce and resharpen. However, the high field spectra just progressively narrow. The difference in the zero field NMR spectra for $\kappa/A = 1$ is great, the width of the broad resonance in Fig. 15 being $6A$. The particular consequences for relaxation will be discussed separately.[35] Zero field NMR is obviously more sensitive to these motions than high field NMR.

D. Conclusions

Zero field NMR is applicable to the study of molecular dynamics. The changes in the spectra involve not only the line shape and width but also the frequency of the resonances. As zero field NMR spectra have "high-resolution" character, they are, in general, more sensitive to subtle changes in exchange rates and motional models. Systems with $\eta \neq 0$ can be identified more precisely due to this high resolution character and should prove extremely useful in the accurate determination of the jump angle for two-site problems and the determination of the orientation of the EFG tensor and exchange rates in many site dynamic problems.

ACKNOWLEDGMENTS

P. Jonsen gratefully acknowledges the support of the UK Science and Engineering Council in providing a post doctoral research fellowship. E. Ohmes is thanked for his work in transferring the diffusion programs to the CRAY 2. G. Kothe acknowledges S. Weissman for providing stimulating discussion concerning dynamics in zero field NMR. This work was supported, in part, by the Director, Office of Energy Research, Office of Basic Energy Sciences, Materials Science Division of the U.S. Department of Energy under Contract No. DE-AC03-76SF00098.

APPENDIX

The frequency matrix elements for an arbitrary orientation of the EFG tensor with respect to the tilt frame (in the convention of Ref. 11) is given by

$$\Omega_{k'q'kq} = \sum_{\substack{q_1,q_3=-k' \\ q_2,q_4=k}}^{k'k} \langle T^M_{k'q_1} | d^{(k')}_{q_1q_3}(\theta) d^{(k)}_{q_2q_4}(\theta) \mathscr{D}^{(k')}_{q_3q_1}(\alpha'\beta'\gamma') \times \mathscr{D}^{(k)}_{q_4q_2}(\alpha'\beta'\gamma') \hat{\mathscr{H}}_Q | T^M_{kq_2} \rangle , \quad \text{(A1)}$$

where the $d^{(k')}_{q'q}(\theta)$ are elements of the kth rank reduced Wigner rotation matrix; the angles $\theta, \alpha'\beta'\gamma'$ being defined in Ref. 11. If the transformations are made as in Ref. 11 which make the special case ($\alpha'\beta'\gamma' = 0$), then the matrix of elements described in Eq. (A1) has real diagonal 4×4 blocks and imaginary off-diagonal 4×4 blocks. This matrix is made totally real, and is diagonalizable to give the correct eigenvalues, by using the following transformation:

$$\begin{aligned} g_{1+} &\equiv i g_{1+} \\ 2^{1/2} g_{10} &\equiv -i 2^{1/2} g_{20} , \\ g_{2-} &\equiv -i g_{2-} , \\ g_{22+} &\equiv i g_{22+} . \end{aligned} \quad \text{(A2)}$$

For the special case ($\alpha'\beta'\gamma' = 0$) of Ref. 11, motion only mixes ($2^{1/2}g_{10}, g_{2+}, g_{22-}, g_{1-}$) of the sites and ($g_{1+}$, $2^{1/2}g_{20}, g_{2-}, g_{22+}$) of the sites. For $\beta' \neq 0$ and $\beta' \neq 90°$, then all the components of magnetization are mixed by motion.

[1]H. W. Spiess, *NMR Basic Principles and Progress*, edited by P. Diehl, E. Fluck, and R. Kosfeld (Springer, Berlin, 1976); J. Chem. Phys. **72**, 6755 (1980).
[2]H. Sillescu, Pure Appl. Chem. **54**, 619 (1982).
[3]P. Meier, E. Ohmes, G. Kothe, A. Blume, J. Weidner, and H.-J. Eibl, J. Phys. Chem. **87**, 4904 (1983).
[4]K. Müller, P. Meier, and G. Kothe, Progr. NMR Spectrosc. **17**, 211 (1985).
[5]J. I. Kaplan and G. Fraenkel, *NMR of Chemically Exchanging Systems* (Academic, New York, 1980).
[6]A. Baram, Z. Luz, and S. Alexander, J. Chem. Phys. **64**, 4321 (1976); Z. Luz, Isr. J. Chem. **23**, 305 (1983).
[7]G. E. Pake, J. Chem. Phys. **16**, 327 (1948).
[8]N. Bloembergen and J. A. Rowland, Acta Metallurg. **1**, 731 (1953).
[9]C. Schmidt, S. Wefing, B. Blümich, and H. W. Spiess, Chem. Phys. Lett. **130**, 84 (1986).
[10]J. W. Hennel, A. Birczynski, S. F. Sagnowski, and M. Stachurowa, Z. Phys. B **60**, 49 (1985).
[11]P. Jonsen, M. Luzar, M. Mehring, and A. Pines, J. Chem. Phys. **85**, 4873 (1986).
[12]Yu. A. Serebrennikov, Chem. Phys. **112**, 253 (1987).
[13]P. Meier, E. Ohmes, and G. Kothe, J. Chem. Phys. **85**, 3598 (1986).
[14]J. H. Freed, G. V. Bruno, and C. Polnaszek, J. Chem. Phys. **55**, 5270 (1971).
[15]D. P. Weitekamp, A. Bielecki, D. Zax, K. Zilm, and A. Pines, Phys. Rev. Lett. **50**, 1807 (1983).
[16]A. Bielecki, J. B. Murdoch, D. P. Weitekamp, D. B. Zax, K. W. Zilm, and H. Zimmermann, J. Chem. Phys. **80**, 2232 (1984).
[17]J. M. Millar, A. M. Thayer, A. Bielecki, D. B. Zax, and A. Pines, J. Chem. Phys. **83**, 934 (1985).
[18]D. B. Zax, A. Bielecki, K. W. Zilm, A. Pines, and D. P. Weitekamp, J. Chem. Phys. **83**, 4877 (1985).
[19]A. Bielecki, D. B. Zax, K. W. Zilm, and A. Pines, Rev. Sci Instrum. **57**, 393 (1986).
[20]R. Kreis, D. Suter, and R. R. Ernst, Chem. Phys. Lett. **118**, 120 (1985).
[21]R. Kubo and T. Toyabe, *Magnetic Resonance and Relaxation*, edited by R. Blinc (North-Holland, Amsterdam, 1967), pp. 810–823; R. Kubo, *Stochastic Processes in Chemical Physics, Advances in Chemical Physics*, edited by K. Shuler (Wiley, New York, 1969), Vol. 16, pp. 101–127.
[22]J. H. Freed, G. V. Bruno, and C. F. Polnaszek, J. Phys. Chem. **75**, 3386 (1971).
[23]J. R. Norris and S. I. Weissman, J. Phys. Chem. **73**, 8119 (1969).
[24]G. Kothe, Mol. Phys. **33**, 147 (1977).
[25]E. P. Wigner, *Group Theory and Its Application to Quantum Mechanics of Atomic Spectra* (Academic, New York, 1959).
[26]L. T. Muus, *Electron Spin Relaxation in Liquids*, edited by L. T. Muus and P. W. Atkins (Plenum, New York, 1972), pp. 1–24.
[27]G. Kothe, K. H. Wassmer, A. Naujok, E. Ohmes, J. Rieser, and K. Wallenfels, J. Magn. Reson. **36**, 425 (1979).
[28]H. Sillescu, J. Chem. Phys. **54**, 2110 (1971).
[29]R. G. Gordon and T. Messenger, *Electron Spin Relaxation in Liquids*, edited by L. T. Muus and P. W. Atkins (Plenum, New York, 1972), pp. 341–381.
[30]R. G. Barnes, *Advances in Nuclear Quadrupole Resonance*, edited by J. A. S. Smith (Heyden, London, 1974), Vol. 1.
[31]A. Weiss and N. Weiden, *Advances in Nuclear Quadrupole Resonance*, edited by J. A. S. Smith (Heyden, London, 1980), Vol. 4; H. Chihara and N. Nakamura, *ibid.*, Vol. 4.
[32]T. Chiba, J. Chem. Phys. **39**, 947 (1963).
[33]B. H. Meier, F. Graf, and R. R. Ernst, J. Chem. Phys. **76**, 767 (1982).
[34]D. T. Edmonds, M. J. Hunt, and A. L. Mackay, J. Magn. Reson. **20**, 505 (1975).
[35]P. Meier and G. Kothe (in preparation).
[36]S. Alexander and A. Tzalmona, Phys. Rev. A **138**, 845 (1965).
[37]O. Pschorn and H. W. Spiess, J. Magn. Reson. **39**, 217 (1980).
[38]S. Vega, Adv. Mag. Reson. **6**, 259 (1973).